

A high heating rate pyrolysis model for the Phenolic Impregnated Carbon Ablator (PICA) based on mass spectroscopy experiments

Francisco Torres-Herrador^{a,b,*}, Jeremie B.E. Meurisse^c, Francesco Panerai^d,
Julien Blondeau^{b,e}, Jean Lachaud^f, Brody K. Bessire^g, Thierry E. Magin^a, Nagi
N. Mansour^h

^a*von Karman Institute for Fluid Dynamics, 1640 Rhode-St-Genese, Belgium*

^b*Thermo and Fluid dynamics (FLOW) Faculty of Engineering, Vrije Universiteit Brussel (VUB), 1050 Brussels, Belgium*

^c*Science and Technology Corporation (STC) at NASA Ames Research Center, CA 94035 Moffett Field, USA*

^d*University of Illinois at Urbana-Champaign, IL 61801 Urbana, US*

^e*Combustion and robust optimization (BURN), Vrije Universiteit Brussel (VUB) and Université Libre de Bruxelles (ULB), 1050 Brussels, Belgium*

^f*University of Bordeaux, 33405 Talence, France*

^g*Analytical Mechanics Associates (AMA) at NASA Ames Research Center, CA 94035 Moffett Field, USA*

^h*NASA Ames Research Center, CA 94035 Moffett Field, USA*

Abstract

A novel model for the pyrolysis of the Phenolic Impregnated Carbon Ablator (PICA) at high heating rate is developed and calibrated based on high fidelity thermal decomposition experiments. The calibration relies on accurate quantification of pyrolysis gases obtained from mass spectroscopy analysis during thermal decomposition at fast heating rates simulating flight conditions. Model calibration is achieved by coupling the Porous material Analysis Toolbox based on OpenFOAM (PATO) with an optimization software (Dakota). A multi-objective genetic algorithm is used to fit the experimental data by optimizing the model parameters for an element and a species-based formulation. The new model captures both the material mass loss and the gaseous species produced during pyrolysis.

Keywords: Carbon/phenolic composite, Kinetics, Thermal degradation

*Corresponding author

Email address: fratorhe@vki.ac.be (Francisco Torres-Herrador)

Highlights

- Developed first pyrolysis model for PICA at high heating rate.
- Devolatilization models calibrated by coupling material solver and genetic optimizer.
- New pyrolysis models reproduce experimental data at flight-like heating rate.
- Model captures both material thermal decomposition and pyrolysis gas production.

Nomenclature

Acronyms		$\mathcal{A}_{i,j}$	Pre-exponential factor [s^{-1}]
DSC	Differential Scanning Calorimetry	$\mathcal{E}_{i,j}$	Activation Energy [$\text{kJ} \cdot \text{mol}^{-1}$]
DTGA	Differential TGA	\mathcal{R}	Universal gas constant [$\text{J} \cdot \text{K}^{-1} \cdot \text{mol}^{-1}$]
GC	Gas Chromatography	\mathcal{S}	Solid
MOGA	Multi Objective Genetic Algorithm	$\tilde{F}_{i,j,k}$	Weighted F parameter [-]
MS	Mass Spectrometry	A_k	Species or elements k
PATO	Porous material Analysis Toolbox based on OpenFOAM	$F_{i,j}$	Fraction density loss [-]
PICA	Phenolic Impregnated Carbon Ablator	I_{A_k}	Fitness function of A_k [K^{-2}]
SOGA	Single Objective Genetic Algorithm	L_{A_k}	Normalized production of A_k [K^{-1}]
STA	Simultaneous Thermal Analysis	m	Mass [kg]
TACOT	Theoretical Ablative Composite for Open Testing	N_g	Number of gases
TGA	Thermogravimetric Analysis	N_P	Number of solid phases
TPS	Thermal Protection System	$n_{i,j}$	Order of the reaction [-]
Greek Symbols		P_i	Solid phases i in solid \mathcal{S}
β	Heating rate [$\text{K} \cdot \text{s}^{-1}$]	$p_{i,j}$	Solid sub-phase in phase P_i
$\chi_{i,j}$	Advancement of the reaction [-]	$R_{i,j}$	Reaction j in phase i
π_{A_k}	Production rate of A_k [$\text{kg} \cdot \text{m}^{-3} \cdot \text{s}^{-1}$]	T	Temperature [K]
ρ	Density [$\text{kg} \cdot \text{m}^{-3}$]	y_{A_k}	Mass fraction of A_k [-]
$\zeta_{i,j,k}$	Mass stoichiometric coefficient [-]	Subscripts	
Roman Symbols		0	Initial conditions
\bar{p}	Optimization variable	∞	Final conditions
		i	Solid phase
		j	Solid sub-phase in phase i
		amb	Ambient conditions

1. Introduction

An organic solid submitted to high temperatures undergoes a thermal decomposition process known as pyrolysis. In this irreversible process, the polymeric chains break up. This leads to the formation of a solid carbonaceous char and to the release of volatile products [1]. Pyrolysis is found in many

thermal engineering processes, including the production of biofuels via biomass decomposition, the burning of wood, the treatment of plastic waste via thermal depolymerization. In this work, we focus on the aerospace application of pyrolysis occurring when the phenolic resin of carbon/phenolic heat shields used in modern entry spacecraft decomposes at high temperature. The mathematical formulation and the methodology described can be generically used in other pyrolysis processes.

During atmospheric entry, the high kinetic energy of the spacecraft is converted into heat by drag due to the shock formed ahead of the vehicle. The temperatures achieved behind the shock (10 000 K) at hypersonic speeds require an efficient Thermal Protection System (TPS) to insulate the spacecraft and protect the payload. In recent years, a new generation of ablative TPS has gained attention due to its applicability to different space exploration missions. These materials are composites made of short carbon fibers binded together in rigid or flexible preform [2] and infused with a phenolic resin [3]. A notable material within the lightweight carbon/resin class is the Phenolic Impregnated Carbon Ablator (PICA) developed by NASA, which has been successfully used in missions such as Mars Science Laboratory (MSL) or on the Stardust Sample Return Capsule (SRC).

PICA has shown excellent thermal protection performances due to several factors. The high porosity of its carbon fiber preform and the high surface area phenolic resin insure high insulation properties. The resin decomposes via a globally endothermic pyrolysis process, producing a flux of pyrolysis gases that partially blocks the incoming heat [4].

Several researchers have studied the thermal degradation of carbon/phenolic composites. The first experimental studies were carried out in the 1960s by Goldstein [5] and Sykes [6]. In the late 1990s, Trick and Saliba [7, 8] developed a first kinetic model for the pyrolysis of a carbon/phenolic ablator. In these studies, the mass loss and the species produced were investigated by means of Thermogravimetric Analysis (TGA) and Gas Chromatography (GC). Milos and co-authors [9, 10, 11] have built ablation models used to size all NASA's

PICA heat shields to date. More recently, Lachaud & Mansour [12] developed a new pyrolysis model by combining information from the aforementioned experiments. However, these studies were carried out at low heating rates ($\beta \approx 10 \text{ K} \cdot \text{min}^{-1}$) that are much lower than experienced during atmospheric entry ($\beta \approx 1800 \text{ K} \cdot \text{min}^{-1}$ MSL MISP5) [13]. Several studies [14, 15] have shown that the extrapolation of kinetic data towards higher heating rates may result in erroneous predictions on the material decomposition.

In material response simulations of carbon/phenolic ablators such as PICA, the degradation state of the material affects effective properties (e.g heat capacity, thermal conductivity) which are commonly computed as a weighted average between a virgin and a fully charred state. Therefore, an accurate modeling of the material degradation state is critical to enable predictive simulation capabilities.

Wong *et al.* [16] performed a series of experiments in which the temperature of the sample is increased by steps of 50 K. At each step, the sample is kept at the target temperature for 1 h and quenched after, so that the gases can be analyzed *a posteriori* by means of GC. This allows the collection of all the gases produced as well as the possibility to measure the mass at every step.

Recently, Bessire and Minton [17] measured 14 significant pyrolysis products of PICA using a mass spectrometric technique. In this technique, samples ($2.5 \times 0.9 \times 0.7 \text{ cm}^3$) are pyrolyzed in vacuum by imposing a voltage across the sample, thus passing an electric current directly through the carbon fiber substrate of the composite material (Joule heating). The phenolic matrix of the composite material is pyrolyzed as the carbon fiber substrate is resistively heated and the gaseous products that evolve from the surface of the material are measured with a mass spectrometer. The technique produced linear heating rates of up to $25 \text{ K} \cdot \text{s}^{-1}$ which is an order of magnitude higher than the heating rates achieved with commercially available TGA's. The technique described by Bessire and Minton allows for the quantitative detection of pyrolysis gases which are then used to construct temperature dependent mass loss curves. Therefore, this approach generates mass loss data while also providing essential insight into the complex thermal decomposition processes that are not revealed through

traditional TGA measurements.

The first part of this paper (Section 2) describes a general formulation of pyrolysis using the multicomponent devolatilization mechanism. In Section 3, we use the formulation to calibrate a pyrolysis model of PICA for high heating rates using an optimization procedure, to the experimental results of Besire and Minton. Both the flow rate and the composition of the pyrolysis gases are predicted. Finally, in Section 4 the developed model has been compared to the model of Lachaud *et al.* which was obtained at low heating rates.

2. Pyrolysis Model

Two models have been developed: one based on species production and another on elemental production rates. The model based on species has been calibrated directly from the data of Bessire and Minton [17]. This model is based on the model of Lachaud and Mansour [12], allowing for the computations of finite-rate chemistry in the gas phase. However, the mechanisms and rate coefficients currently used for finite-rate chemistry are not well established [18].

Consequently, a model based on the elemental composition has also been developed. This model takes into account the hypothesis that inside a porous media, the gases reach thermo-chemical equilibrium at a rate which is much faster than the convection time scale [18]. In such case, only the elemental composition of the gas mixture is needed and the equilibrium species composition of the mixture can be obtained by minimizing the Gibbs free energy equation for a given set of species [19]. Therefore, the elemental mass production rates have been derived from the experimental MS results of Bessire [17] and kinetic parameters have been calibrated for this model.

2.1. General formulation

Pyrolysis is a complex process which has been modeled using different approaches [20]. In this work, pyrolysis modeling is addressed using a multicomponent devolatilization mechanism [18], also known as parallel kinetic model.

This model assumes that a solid \mathcal{S} is composed of N_P different phases. Each phase P_i may be composed of sub-phases $p_{i,j}$. A sub-phase $p_{i,j}$ undergoes a pyrolysis reaction that releases gases A_k in a proportion given by mass stoichiometric coefficients $\zeta_{i,j,k}$. The released gases can be either treated as elements or species, depending on the formulation chosen. The remaining solid after the completion of pyrolysis is known as char. This model can be formulated as:

$$\mathcal{S} \rightarrow \sum_i^{N_P} \sum_j^{N_{P_i}} p_{i,j} \quad (1)$$

$$p_{i,j} \xrightarrow{R_{i,j}} \sum_k^{N_*} \zeta_{i,j,k} A_k, \quad * \begin{cases} e = \text{elements} \\ s = \text{species} \end{cases} \quad (2)$$

Each reaction $R_{i,j}$ is modeled using an Arrhenius-like equation, of the following form:

$$\frac{d\chi_{i,j}}{dt} = \mathcal{A}_{i,j} (1 - \chi_{i,j})^{n_{i,j}} \exp\left(\frac{-\mathcal{E}_{i,j}}{\mathcal{R}T}\right), \quad (3)$$

where the advancement of reaction ($\chi_{i,j} \in [0, 1]$) evolves as function of the kinetic parameters ($\mathcal{A}_{i,j}$, $\mathcal{E}_{i,j}$, $n_{i,j}$) and the temperature (T).

The initial –virgin– density of the solid ($\rho_{s,0}$) is expressed as the sum of the density of each phase ($\rho_{i,0}$) weighted by its volume fraction ($\epsilon_{i,0}$):

$$\rho_{s,0} = \sum_i^{N_P} \epsilon_{i,0} \rho_{i,0} \quad (4)$$

The density evolution of the solid can be computed as the contribution of each advancement of reaction $\chi_{i,j}$ scaled by the fraction density loss $F_{i,j}$ [18]. This constant expresses the fraction of density that is lost when reaction $R_{i,j}$ reaches completion (i.e $\chi_{i,j} = 1$):

$$\rho_s(t) = (\rho_{s,0} - \sum_i^{N_P} \sum_j^{N_{P_i}} \epsilon_{i,0} \rho_{i,0} \chi_{i,j} F_{i,j}) \quad (5)$$

Similarly, the gas production rate of A_k (element or species) can be expressed as:

$$\pi_{A_k} = \sum_i^{N_P} \sum_j^{N_{P_i}} \rho_{i,0} F_{i,j} \zeta_{i,j,k} \frac{d\chi_{i,j}}{dt} \quad (6)$$

Using multicomponent volatilization mechanisms, one may assume that products that have production peaks at the same temperature, are produced by the same reaction and can thus be grouped.

In the present study, only the phenolic resin of PICA decomposes via pyrolysis, thus the subscript for the phases $i = 1$ will be omitted in what follows for simplicity.

2.2. Species-based model

For the production of species, we propose a kinetic scheme made of 6 reactions, as shown in Fig. 1. The scheme is based on the species production quantified during PICA pyrolysis experiments by Bessire and Minton [17]. Results from the experimental data at 6.1 K/s are shown in Fig. 2. Six production maxima are identified, labeled as “ R_i ” in the figure. Two low temperature (<450 K) peaks capture the early production of water, CO, CO₂ and the two C₃H₈O isomers. Peaks for the bulk of production of permanent gases, alcohols and aromatics are concentrated in the 600-800 K range. A final minor peak is included to capture a delayed production in H₂ and CO near 1100 K.

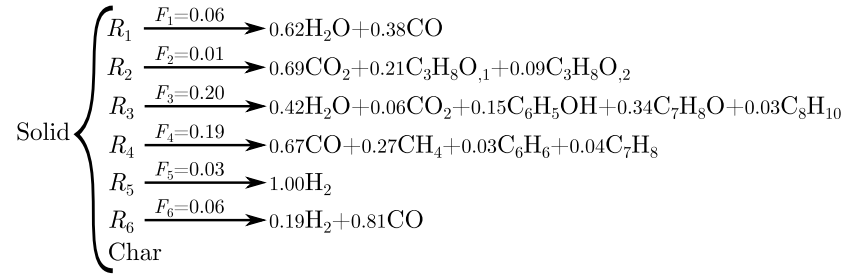


Figure 1: Kinetic scheme proposed for the species model decomposition

Of the 14 species measured by Bessire and Minton, dimethylphenol and trimethylphenol were not found in the NASA-7 [19] database used in this study. It was decided to group the contributions of the two missing species to that of cresol, which is chemically similar [21]. It is also noted that the mass contribution of those species is negligible compared to other compounds.

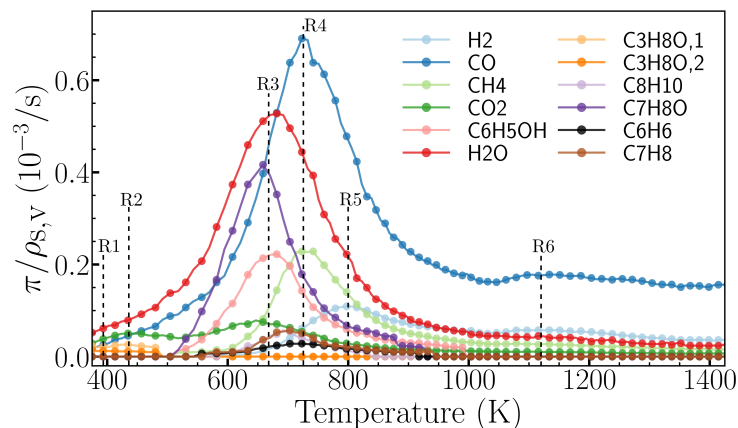


Figure 2: Experimental measurements of Bessire and Minton grouped by production peaks

With this scheme, we have 6 kinetic triplets (\mathcal{E} , \mathcal{A} , n) and 17 weighted- F ($\tilde{F}_{j,k}$) parameters, thus 35 constants to be determined.

2.3. Element-based model

Our second case uses a model that tracks the elements from the pyrolysis gases of PICA. The SC1008 phenolic resin is composed of polymeric chains made of carbon, hydrogen and oxygen. All the compounds detected by Bessire and Minton [17] are combinations of these three elements. The elemental fractions can be computed by adding the contributions of the 14 species measured experimentally. The elemental model is built based on previous studies on the pyrolysis of PICA which was described by four reaction stages [7, 22, 23]. The kinetic scheme is depicted in Figure 3. The third reaction (R_3) consumes most of the phenolic resin in this model.

2.4. Numerical implementation

A 0D pyrolysis reactor model was developed in the Porous material Analysis Toolbox based on OpenFOAM (PATO) [18]. PATO is an open source software developed at NASA to study the thermal degradation of porous materials like PICA [18]. From OpenFOAM, PATO inherits the numerical schemes, the architecture and the typical case-folder structure. The modular architecture of

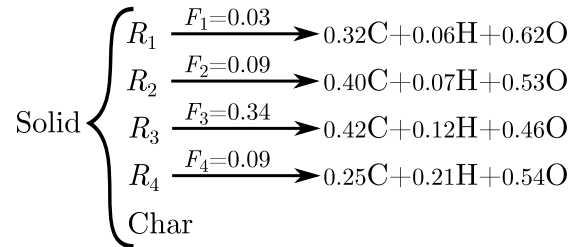


Figure 3: Kinetic scheme proposed for the element model decomposition.

PATO allows the selection of determined modules that address the physics of interest. In this study, the pyrolysis module that implements the model presented in Section 2 was used.

Considering the devolatilization mechanism previously presented, the production of each species A_k in the reaction $R_{i,j}$ can be assumed to be independent, and the use of stoichiometric coefficients can be replaced for k reactions which keep the same kinetic triplet $(\mathcal{A}_{i,j}, \mathcal{E}_{i,j}, n_{i,j})$, a weighted F parameter \tilde{F} such that

$$\tilde{F}_{i,j,k} = \zeta_{i,j,k} F_{i,j} \quad (7)$$

This allows to decouple the problem and removes the need of adding a unit sum constraint to the stoichiometric coefficient $(\sum_k^{N_*} \zeta_{i,j,k} = 1)$, which could be a difficult optimization constraint for reactions producing more than two gases. The original $F_{i,j}$ can be then re-computed from its weighted components as $F_{i,j} = \sum_k^{N_*} \tilde{F}_{i,j,k}$. Finally, the stoichiometric coefficients $\zeta_{i,j,k}$ can be calculated as $\zeta_{i,j,k} = \tilde{F}_{i,j,k} / F_{i,j}$, satisfying the original unity sum constraint.

3. Calibration Methodology

Using the parallel reactions scheme, the decomposition model could be fully decoupled. We recall the omission of the subindex i for simplicity as mentioned in the previous section. Each reaction was composed of a kinetic triplet (E_j, A_j, n_j) and a fraction sub-species $(\tilde{F}_{j,k})$. This resulted in 24 and 35 unknown parameters to be calibrated for the case of the elements (4 reactions) and the

species (6 reactions), respectively.

In order to carry out the minimization process, PATO was interfaced with Dakota, an open source software developed by Sandia National Laboratories for optimization and uncertainty quantification [24]. Dakota provides several optimization algorithms, including gradient-based, genetic and surrogate-based methods. For the present work we used Genetic Algorithms (GA) [25], both single and multi objective, which combined a robust formulation to an efficient parallel implementation for the specific problem investigated.

A flowchart of the minimization process is presented in Figure 4. A user-defined number of individuals –population– is first generated. It is an aleatory combination of possible values of the unknown parameters in their search space. Each set of parameters is then provided as input to PATO, which computes the solution of the pyrolysis model. The goodness of fit is evaluated by comparison to experimental data using a least squares method.

Neglecting changes in volume, the formulation presented previously can be expressed in terms of mass. An appropriate normalization was carried out in order to obtain consistency between experimental data and simulations. Indeed, the optimization had to be robust and consistent with the mass contribution of each species. To this end, we considered the mass fraction y_{A_k} of species/element:

$$y_{A_k}(T) = \frac{\int \pi_{A_k} dT}{\sum_k^{N_g} \int \pi_{A_k} dT} = \frac{m_{A_k}(T)}{m_{\text{gas}}(T)} \quad (8)$$

and the derivative of the total mass loss:

$$\begin{aligned} \text{DTGA} &= -\frac{d\left(\frac{m_s(T)}{m_{s,0}}\right)}{dT} = -\frac{1}{m_{s,0}} \frac{d\left(1 - \sum_{k=1}^{N_g} m_{A_k}(T)\right)}{dT} \\ &= \frac{1}{m_{s,0}} \frac{d(m_{\text{gas}}(T))}{dT}. \end{aligned} \quad (9)$$

Here, y_{A_k} provides information on the relative importance of each generated product, while DTGA provides information on the actual gas production and sensitivity to the optimization. Their product, $y_{A_k} \cdot \text{DTGA}$, defines the relative

mass production rate per unit temperature, which is used to compare the 0D model and the experiments.

Then, the algorithm minimized the following fitness function:

$$I_{A_k} = \sum_{l=1}^n (L_{A_k,l}^{\text{exp}} - L_{A_k}^{\text{PATO},l})^2 \quad (10)$$

where $L_{A_k}^{\text{exp}}$ and $L_{A_k,l}^{\text{PATO},l}$ are respectively the normalized experimental and simulated data points for the production of each gas. Thus, the sum over the n data point provides the squared residuals for a given gas A_k .

At each iteration of the GA, the solution will move towards the optimal solution by combinations of the most optimal designs (reproduction) and random changes (mutations) that ensure the exploration of the entire search space. As opposed to gradient-based methods the GA provides a global minimum rather than a local one.

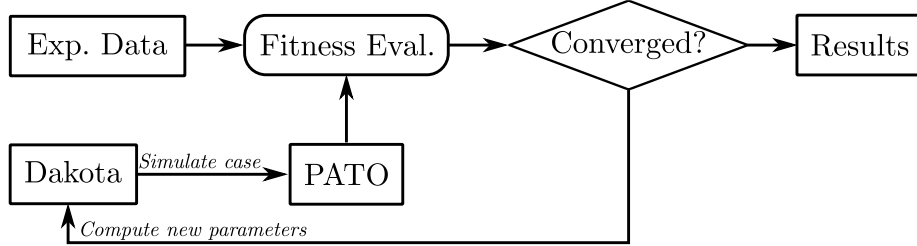


Figure 4: Flowchart of the minimization routine

To carry out the optimization, we used both the multi-objective (MOGA) and single objective (SOGA) genetic algorithm implementations available in Dakota. To eliminate local minima for the genetic optimization (SOGA) we performed a preliminary calibration for each input independently, providing a first approximation to the optimum and narrowing the search space of each parameter. MOGA was subsequently used for the bulk of the optimization process. It was observed that in order to improve convergence, it was convenient to non-dimensionalize the search space of the variables $p = [p_{\text{low}}, p_{\text{high}}]$ such that $\bar{p} = [0, 1]$. For the pre-exponential factor, a logarithmic scaling was applied.

The inputs for MOGA are summarized in Table 1. The large population size (600) was selected due to the high dimensionality of the problem, based on the work by Gotshall & Rylander [26]. The large crossover and mutation rates ensured the coverage of the search space. The convergence criterion selected to stop if in 10 consecutive generations of the algorithm, the fittest individual did not change in a 0.05%.

Table 1: Options used in the optimization MOGA of DAKOTA

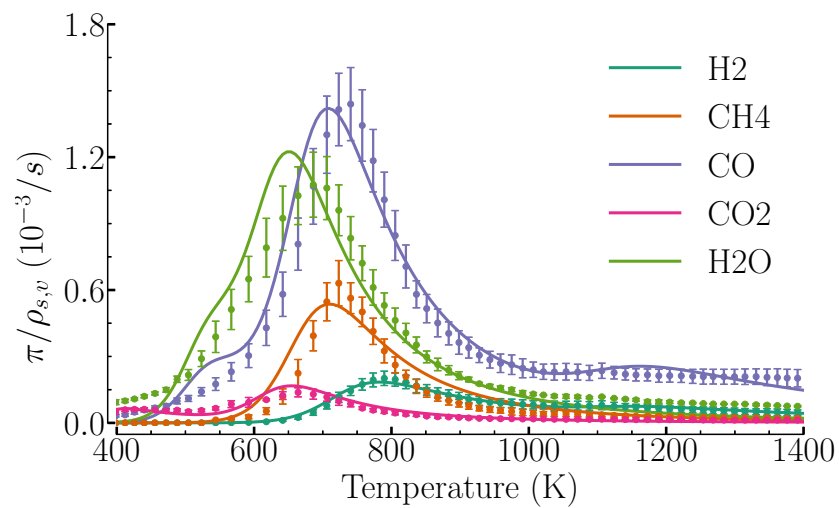
fitness_type	domination_count
population_size	600
replacement_type	unique_roulette_wheel
crossover_type	shuffle_random
crossover_rate	0.85
mutation_type	replace_uniform
mutation_rate	0.35

4. Results

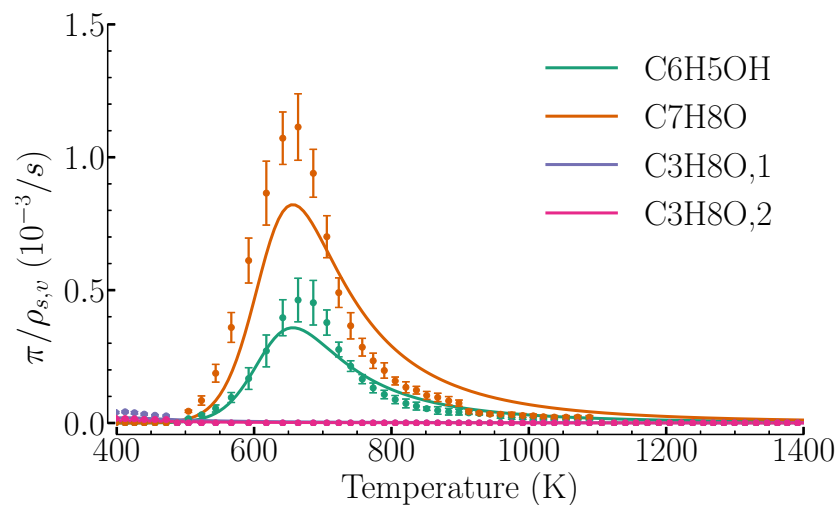
In this section, we present the results obtained for the parameter calibration for the two cases studied (species and elements) as well as a comparison of these models with the one developed by Lachaud *et al.*[18].

4.1. Species-based model

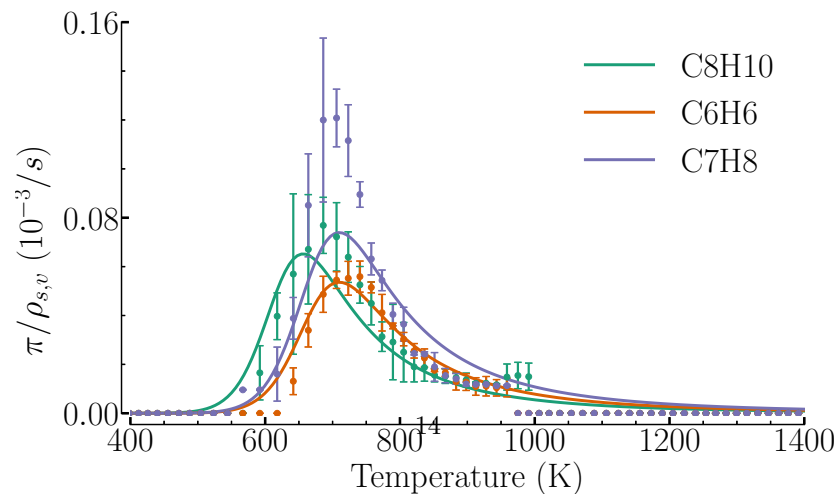
Fig. 5 shows the results of the parameter calibration. It can be observed that simulated values closely follow the experimental data of Bessire and Minton [17]. Gases with higher production rates (permanent gases), have a better fit than those with lower production rates (aromatics).



(a) Permanent



(b) Alcohols



(c) Aromatics

Figure 5: Results from the parameter calibration for the species model. Simulations (—) show good agreement with Experiments (●). The error-bars represent 1σ experimental uncertainty.

The TGA curve was reconstructed from the gas production rate data and compared with that computed by Bessire and Minton (Fig. 6). Although our TGA curve slightly overestimates the mass loss, it is well contained within the standard deviation σ of the experiments over the entire temperature range.

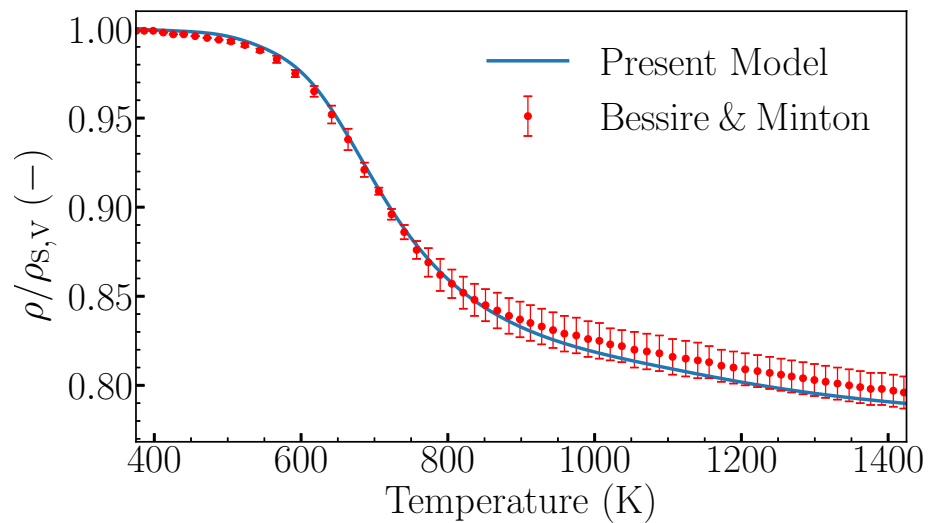


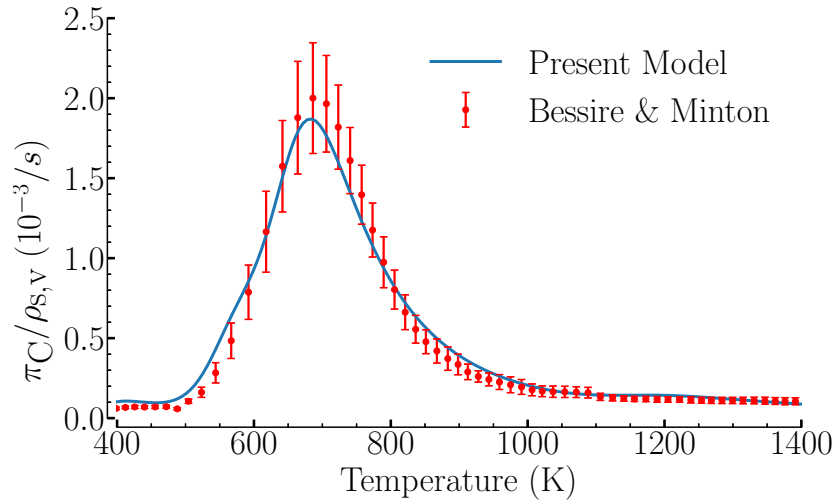
Figure 6: Reconstructed TGA curve for the species model. The error-bars represent 1σ experimental uncertainty.

Table 2: Summary of the kinetic parameters identified for the species-based model.

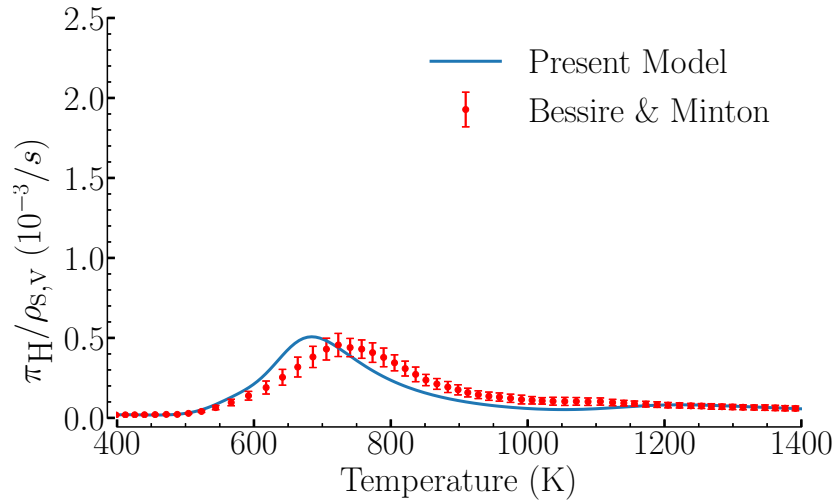
R	$F(-)$	$\log(\mathcal{A})(s^{-1})$	$\mathcal{E}(\text{kJ/mol})$	$n (-)$	$\zeta(-)$
1	0.060	6.59	77.6	5.65	H ₂ O 0.62
					CO 0.38
2	0.009	6.96	61.3	9.96	CO ₂ 0.69
					C ₃ H ₈ O _{,1} 0.21
					C ₃ H ₈ O _{,2} 0.09
3	0.203	6.71	95.1	4.23	H ₂ O 0.42
					CO ₂ 0.06
					C ₆ H ₅ OH 0.15
					C ₇ H ₈ O 0.34
					C ₈ H ₁₀ 0.03
4	0.187	6.67	103.0	4.38	CO 0.67
					CH ₄ 0.27
					C ₆ H ₆ 0.03
					C ₇ H ₈ 0.04
5	0.026	6.58	113.9	6.68	H ₂ 1.00
6	0.059	6.35	175.2	8.85	H ₂ 0.19
					CO 0.81

4.2. Element-based model

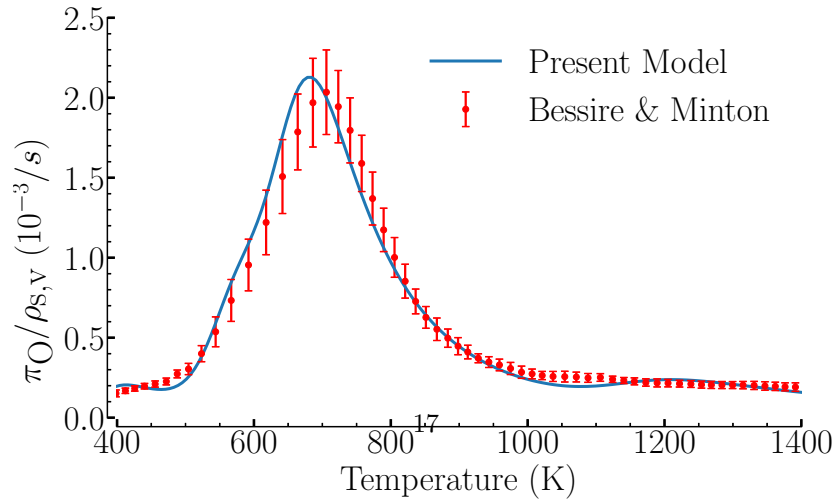
Figures 7 and 8 show the results of the parameter calibration for the elemental model. It can be observed that an excellent fit was found for both C and O. H instead was less accurately captured, as the fitness function tends to favor the elements with higher production rate. As in the case of the species, the reconstructed mass loss curve (TGA) is again accurately computed.



(a) Carbon



(b) Hydrogen



(c) Oxygen

Figure 7: Results from the parameter calibration for the elements model. Simulations (—) show good agreement with Experiments (●). The error-bars represent 1σ experimental

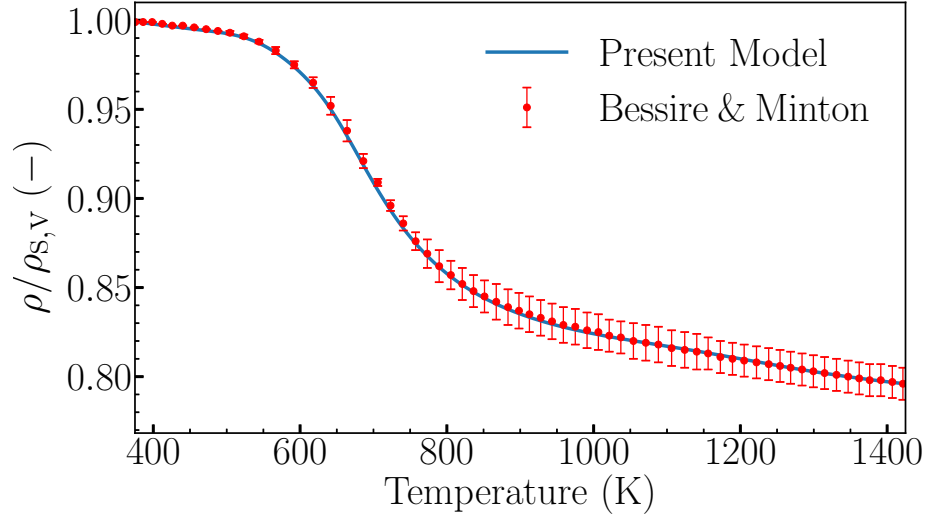


Figure 8: Reconstructed TGA curve for the elements model. The error-bars represent 1σ experimental uncertainty [17].

Table 3: Summary of the kinetic parameters identified for the element-based model.

R	$F(-)$	$\log(\mathcal{A})(s^{-1})$	$\mathcal{E}(kJ/mol)$	$n (-)$	$\zeta(-)$
1	0.032	5.67	51.4	7.74	C 0.32
					H 0.06
					O 0.62
2	0.089	7.02	87.4	4.02	C 0.40
					H 0.07
					O 0.53
3	0.336	7.03	103.7	4.33	C 0.42
					H 0.12
					O 0.46
4	0.086	6.9	194.4	9.25	C 0.25
					H 0.21
					O 0.54

4.3. Model comparison in 0D

First, the developed two models (elemental and species based) and the model of Lachaud *et al.* are compared against experimental data from two different sources: Bessire and Minton $6.1 \text{ K} \cdot \text{s}^{-1}$ [17] and Wong *et al.* at $10 \text{ K} \cdot \text{min}^{-1}$ [16].

Figure 9 shows that the developed models accurately describe the experiments of Minton and Bessire at $6.1 \text{ K} \cdot \text{s}^{-1}$ from where they calibrated.

However, at low heating rates, none of the models is capable of reproducing the experiments of Wong *et al.* The mass loss at low heating rates occurs at higher temperatures than the mass loss at high heating rates. This effect cannot be captured by the current devolatilization mechanisms used in aerospace. Nevertheless, such low heating rates are not really representative of an actual re-entry scenario. As shown in Section 4.4, heating rates of $\sim 10 \text{ K} \cdot \text{min}^{-1}$ are only achieved some millimeters from the back surface, while most of the material decomposes at much higher heating rates.

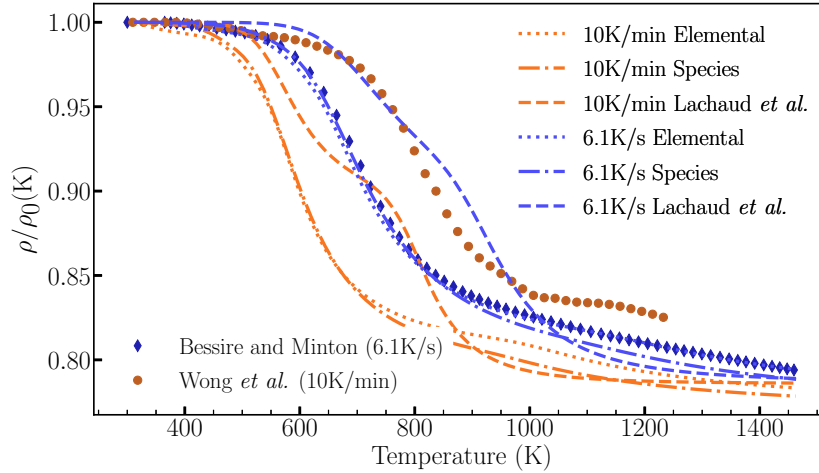


Figure 9: Comparison between proposed elemental model and experiments of Bessire and Minton at different heating rates.

A second comparison is performed between the developed elemental model and the experimental data of Bessire and Minton at 3.1, 6.1, 12.7 and 25.0

$\text{K} \cdot \text{s}^{-1}$ [17].

Figure 10 shows a comparison between the proposed elemental model and the experimental data of Minton and Bessire at heating rates of 3.1, 12.7, and 25 K/s, other than the 6.1 K/s rate used for the present fitting. While we observe a reasonable agreement with the final density loss, our model predicts a shift in the decomposition curves towards higher T for increasing β , in contrast to the experiments where the curves slightly shift towards the lower temperatures. The analysis of Bessire and Minton attributed the heating-rate dependent behavior to competing cross-linking and polymer breakdown processes, the latter becoming increasingly more effective with increasing heating rates. This effect cannot be captured by the current volatilization mechanism, but requires a more sophisticated rate model, requires further developments that are beyond the scope of this paper. Analogous results were observed for the species based model.

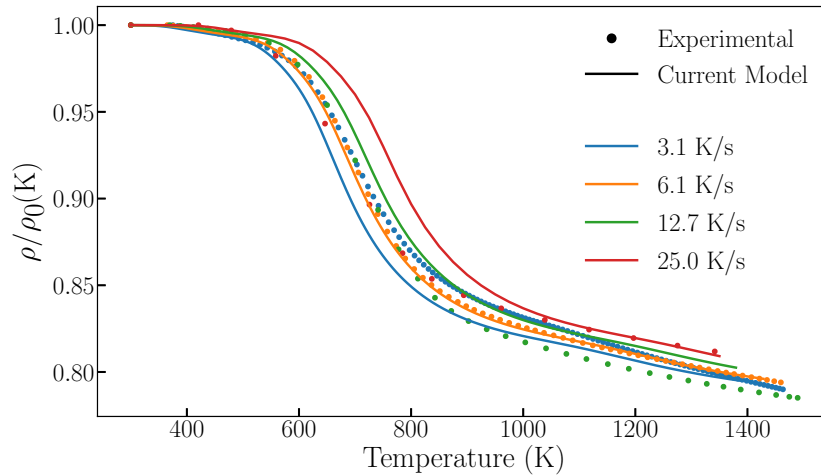


Figure 10: Comparison of models against experimental data in 0D pyrolysis reactor.

4.4. Application to Ablation Test Case #2

A comparison between the elements-based model developed in this work and the one by Lachaud *et al.* [18] is presented in this section. The main

differences between the two models are the source of experimental data used for the calibration and the heating rates at which they were measured. The model of Lachaud *et al.* was derived from old experiments on phenolic resin at slow heating rates ($\approx 10 \text{ K} \cdot \text{min}^{-1}$) [6, 5, 7, 8]. Here we used Bessire and Minton data at $6.1 \text{ K} \cdot \text{s}^{-1}$.

The comparison was carried out using the Ablation Test Case #2 [27]. In this simulation a 1D slab of the Theoretical Ablative Composite for Open Testing (TACOT) material is exposed to a convective BC defined by the heat transfer Stanton number (C_H) as illustrated in Figure 11.

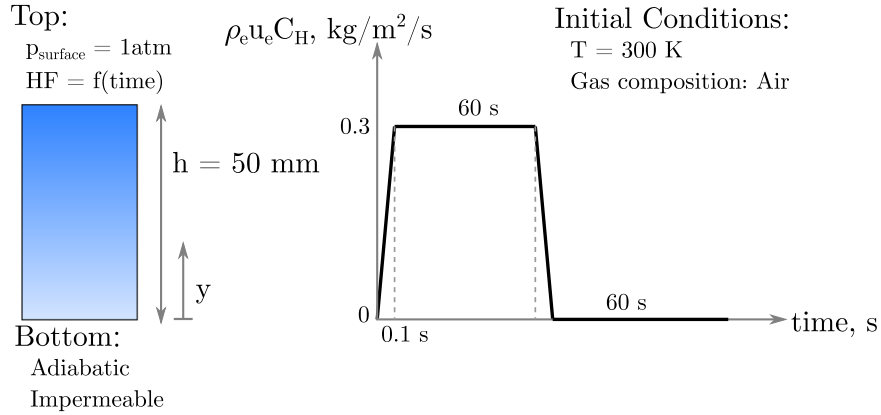


Figure 11: Simulation setup for pyrolysis model comparison based on Ablation Test Case #2 [27].

Figure 12 shows the temperature evolution for the 1D slab. Temperature probes are located at different depths within the material. The black lines show the heating rates at which both models were calibrated.

One can observe that the material temperature evolves similarly in the two models. This is due to the fact that the temperature in this test case is driven by conduction and the effective thermal conductivity.

The small differences in temperature observed are mainly due to the extent of pyrolysis which affects the evolution of the heat capacity of the material. It can be seen in Figure 13 that at the location of the in-depth temperature probes, the density loss of the new elemental model is higher compared to the one computed

with the model of Lachaud *et al.* Since the model of Lachaud was calibrated at low heating rates ($\beta = 10 \text{ K} \cdot \text{min}^{-1}$), the extrapolation towards higher rates shifts the decomposition towards higher temperatures which are never reached at the locations of TC6 and TC7. Therefore, the predicted mass loss is lower than with the proposed model for the upper curves.

The final density loss after completion of pyrolysis of the two models is comparable ($\sim 20\%$) as observed in TC4 and TC5, which is consistent with the final residual mass measured by different authors using the same material, ranging between 77-83% [6, 5, 16, 17].

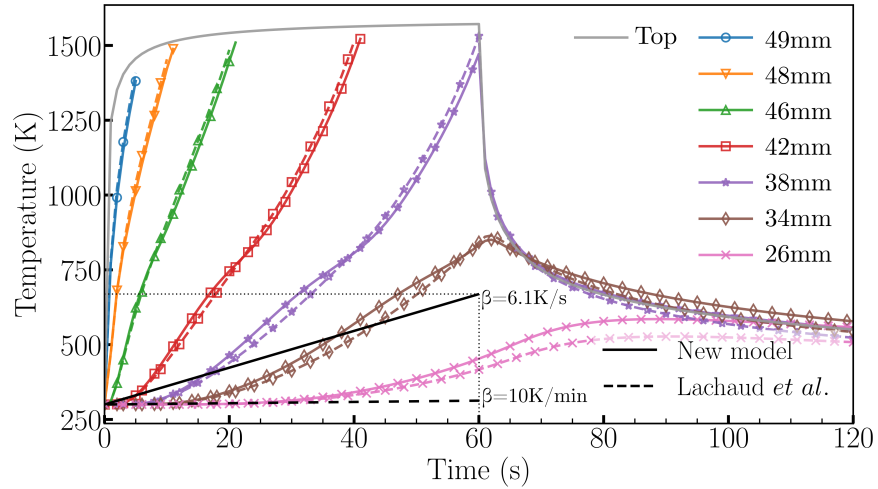


Figure 12: Temperature profile comparison at different depths for the 1D TACOT slab test case. Solid line: developed element model (Table 3), dashed line: model of Lachaud *et al.*[18]. Temperature trace locations in the legend are computed from the bottom of the sample.

It should be noticed that the highest heating rate observed in the test case, close to the surface of the slab, is still significantly higher than the heating rate for which is model has been calibrated $\beta = 6.1 \text{ K} \cdot \text{s}^{-1}$. This is however the highest heating rate for which experimental data is currently available.

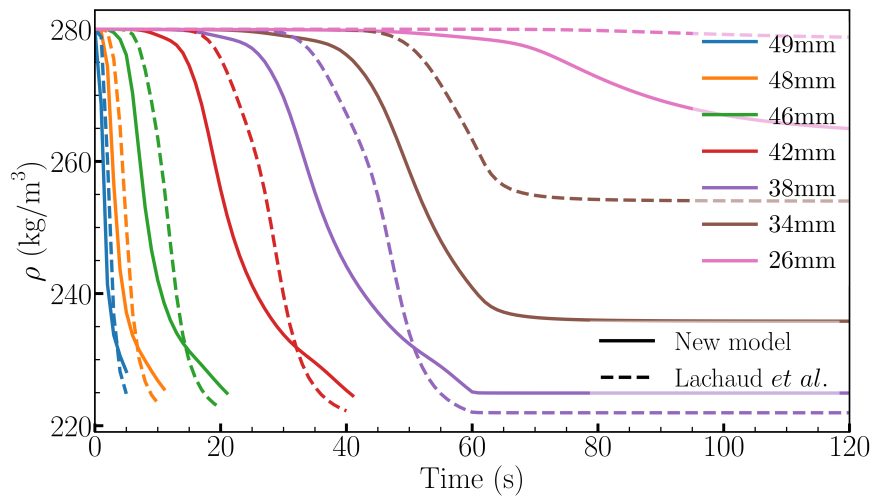


Figure 13: Density profile comparison at different depths for the 1D TACOT slab. Solid line: developed element model (Table 3), dashed line: model of Lachaud *et al.*[18]. Temperature trace locations in the legend are computed from the bottom of the sample.

5. Conclusion

In this work, we have developed two models for high heating rate pyrolysis of PICA: one based on species production, and another based on elemental composition production by coupling the optimization toolbox Dakota to the porous material response solver PATO.

The presented calibration methodology is capable of reproducing the experimental results of Bessire and Minton. Generally, gases with higher mass production rate are favored by the optimization algorithm, achieving a better accuracy than those with lower production rates.

The mass loss profile was reconstructed from the production rates for the two developed models. In both cases, it shows great agreement between the experiments and the calibrated parameters. This is particularly important, since key design variables such as the porosity, the thermal conductivity or the heat capacity of the composite depend on the advancement of reaction since they are weighted averages of virgin and charred states. In addition, this will allow a more accurate prediction of the pyrolysis gases that are blown into the boundary

layer.

Comparing the two new developed models, one can observe better goodness of fit in the elemental model. This is mainly due to two reasons: the lesser number of parameters to be optimized in the case of the elements, which makes it easier for the algorithm to find an accurate result and the grouping of reactions in the kinetics scheme, which gives higher relevance to the species/elements that are produced more abundantly.

Comparison between the new elemental model and the model of Lachaud *et al.* shows that the temperature evolution remains almost unaffected by using the new pyrolysis model except at the deepest thermocouple. However, the density evolution is different. Nevertheless, moving to a more physics-based model requires to re-calibrate the properties of the complete model, for example, the thermal conductivity or the heat capacity.

These new models, calibrated at high heating rate, are more representative of the conditions found during a real application. Extrapolation towards higher heating rates should be carefully considered, and model validation at those heating rates should be carried out when accurate data is available.

Pyrolysis models obtained with the calibration technique developed in this work can be applied to perform practical material response simulation of ablators, such as analyses of arc jet experiments or flight test data. The development of in-situ measurement techniques to quantify pyrolysis species production within charring ablators would allow validating model accuracy under actual aerothermal conditions.

Acknowledgments

The research of F. Torres Herrador is supported by SB PhD fellowship 1S58718N of the Research Foundation Flanders (FWO).

This work is supported by the Entry Systems Modeling project (M. J. Wright project manager, M. D. Barnhardt principal investigator) as part of the NASA Game Changing Development program.

Gregory Pinaud (ArianeGroup) is acknowledged for the fruitful discussions on the modeling of pyrolysis.

We would like to thank Pr. Contat-Rodrigo (Universitat Politècnica de València) for her guidance on the thermal analysis of decomposing materials.

References

- [1] J. Blondeau, H. Jeanmart, Biomass pyrolysis at high temperatures: Prediction of gaseous species yields from an anisotropic particle, *Biomass and Bioenergy* 41 (2012) 107–121. doi:10.1016/j.biombioe.2012.02.016.
URL <http://www.sciencedirect.com/science/article/pii/S0961953412001043>
- [2] F. Panerai, J. C. Ferguson, J. Lachaud, A. Martin, M. J. Gasch, N. N. Mansour, Micro-tomography based analysis of thermal conductivity, diffusivity and oxidation behavior of rigid and flexible fibrous insulators, *International Journal of Heat and Mass Transfer* 108 (2017) 801–811.
- [3] J. C. Ferguson, F. Panerai, J. Lachaud, N. N. Mansour, Theoretical study on the micro-scale oxidation of resin-infused carbon ablators, *Carbon* 121 (2017) 552–562.
- [4] G. Duffa, *Ablative Thermal Protection Systems Modeling*, American Institute of Aeronautics and Astronautics, 2013.
- [5] H. E. Goldstein, Pyrolysis Kinetics of Nylon 6–6, Phenolic Resin, and Their Composites, *Journal of Macromolecular Science: Part A - Chemistry* 3 (4) (1969) 649–673. doi:10.1080/10601326908053834.
URL <http://dx.doi.org/10.1080/10601326908053834>
- [6] G. F. Sykes, *Decomposition Characteristics of a Char-Forming Phenolic Polymer Used for Ablative Composites.*, Tech. Rep. TN D-3810 (1967).
- [7] K. A. Trick, T. E. Saliba, Mechanisms of the pyrolysis of phenolic resin in a carbon/phenolic composite, *Carbon* 33 (11) (1995) 1509–1515.

doi:10.1016/0008-6223(95)00092-R.

URL <http://www.sciencedirect.com/science/article/pii/S000862239500092R>

- [8] K. A. Trick, T. E. Saliba, S. S. Sandhu, A kinetic model of the pyrolysis of phenolic resin in a carbon/phenolic composite, *Carbon* 35 (3) (1997) 393–401. doi:10.1016/S0008-6223(97)89610-8.

URL <http://www.sciencedirect.com/science/article/pii/S0008622397896108>

- [9] F. S. Milos, Y.-K. Chen, M. Congdon, J. M. Thornton, Mars Pathfinder Entry Temperature Data, Aerothermal Heating, and Heatshield Material Response, *Journal of Spacecraft and Rockets - J SPACECRAFT ROCKET* 36 (1999) 380–391. doi:10/cd3xtz.

- [10] F. S. Milos, R. Brewer, Y. Chen, T. Squire, Analysis of Galileo Probe Heatshield Ablation and Temperature Data, *Journal of Spacecraft and Rockets - J SPACECRAFT ROCKET* 36 (1999) 298–306. doi:10/fb3phw.

- [11] M. J. Wright, F. S. Milos, P. Tran, Afterbody Aeroheating Flight Data for Planetary Probe Thermal Protection System Design, *Journal of Spacecraft and Rockets* 43 (5) (2006) 929–943. doi:10/cfqkxp.

URL <https://arc.aiaa.org/doi/10.2514/1.17703>

- [12] J. Lachaud, N. N. Mansour, Porous-material analysis toolbox based on openfoam and applications, *Journal of Thermophysics and Heat Transfer* 28 (2) (2014) 191–202.

- [13] J. B. E. Meurisse, J. Lachaud, F. Panerai, C. Tang, N. N. Mansour, Multidimensional material response simulations of a full-scale tiled ablative heatshield, *Aerospace Science and Technology* 76 (2018) 497–511. doi:10/gc4pgh.

URL <http://www.sciencedirect.com/science/article/pii/S1270963817323179>

- [14] R. K. Agarwal, On the use of the arrhenius equation to describe cellulose and wood pyrolysis, *Thermochimica Acta* 91 (1985) 343–349. doi:10.1016/0040-6031(85)85227-8.
URL <http://www.sciencedirect.com/science/article/pii/S0040603185852278>
- [15] P. Šimon, Isoconversional methods, *Journal of Thermal Analysis and Calorimetry* 76 (1) (2004) 123. doi:10.1023/B:JTAN.0000027811.80036.6c.
URL <https://link.springer.com/article/10.1023/B:JTAN.0000027811.80036.6c>
- [16] H.-W. Wong, J. Peck, J. Assif, F. Panerai, J. Lachaud, N. N. Mansour, Detailed analysis of species production from the pyrolysis of the Phenolic Impregnated Carbon Ablator, *Journal of Analytical and Applied Pyrolysis* 122 (2016) 258–267. doi:10/f9h46d.
URL <http://www.sciencedirect.com/science/article/pii/S016523701630211X>
- [17] B. K. Bessire, T. K. Minton, Decomposition of Phenolic Impregnated Carbon Ablator (PICA) as a Function of Temperature and Heating Rate, *ACS Applied Materials & Interfaces* 9 (25) (2017) 21422–21437. doi:10.1021/acsami.7b03919.
URL <http://dx.doi.org/10.1021/acsami.7b03919>
- [18] J. Lachaud, J. B. Scoggins, T. E. Magin, M. G. Meyer, N. N. Mansour, A generic local thermal equilibrium model for porous reactive materials submitted to high temperatures, *International Journal of Heat and Mass Transfer* 108, Part B (2017) 1406–1417. doi:10.1016/j.ijheatmasstransfer.2016.11.067.
- [19] J. B. Scoggins, J. Rabinovitch, B. Barros-Fernandez, A. Martin, J. Lachaud, R. L. Jaffe, N. N. Mansour, G. Blanquart, T. E. Magin, Thermodynamic properties of carbon–phenolic gas mixtures, *Aerospace Science and*

Technology 66 (2017) 177–192. doi:10.1016/j.ast.2017.02.025.

URL <http://www.sciencedirect.com/science/article/pii/S1270963816307945>

- [20] C. Di Blasi, Modeling chemical and physical processes of wood and biomass pyrolysis, *Progress in Energy and Combustion Science* 34 (1) (2008) 47–90. doi:10.1016/j.pecs.2006.12.001.

URL <http://www.sciencedirect.com/science/article/pii/S0360128507000214>

- [21] B. Bessire, private communication.

- [22] W. M. Jackson, R. T. Conley, High temperature oxidative degradation of phenol–formaldehyde polycondensates, *Journal of Applied Polymer Science* 8 (5) (1964) 2163–2193. doi:10.1002/app.1964.070080516.

URL <https://onlinelibrary.wiley.com/doi/abs/10.1002/app.1964.070080516>

- [23] J. A. Parker, E. L. Winkler, The effects of molecular structure on the thermochemical properties of phenolics and related polymers, Tech. Rep. R-276, National Aeronautics and Space Administration, Washington, D.C., oCLC: 55893483 (1967).

- [24] B. M. Adams, L. Bauman, W. J. Bohnhoff, K. R. Dalbey, M. Ebeida, J. P. Eddy, M. S. Eldred, P. Hough, K. Hu, J. Jakeman, J. Stephens, L. P. Swiler, D. Vigil, T. Wildey, DAKOTA : a multilevel parallel object-oriented framework for design optimization, parameter estimation, uncertainty quantification, and sensitivity analysis. Version 6.7, user’s reference manual., Tech. Rep. SAND2014-4633, Sandia National Laboratories (Nov. 2017). doi:10.2172/991841.

- [25] J. Nocedal, S. Wright, *Numerical Optimization*, Springer Science & Business Media, 2006.

- [26] S. Gotshall, B. Rylander, Optimal population size and the Genetic Algorithm.
- [27] J. Lachaud, A. Martin, T. van Eekelen, I. Cozmuta, Ablation Test Case 2, in: 5th Ablation Workshop, Lexington, Kentucky, 2012.